Pergamon

Int. J. Multiphase Flow Vol. 24, No. 3, pp. 499–521, 1998

Printed in Great Britain
PII: S0301-9322(97)00065-7
0301-9322/98 $19.00 + 0.00

BOUNDARY LAYER MODELING OF GRANULAR FLOW IN THE TRANSVERSE PLANE OF A PARTIALLY FILLED ROTATING CYLINDER

A. A. BOATENG

Fuel and Combustion Technology International, Inc., 283 Great Valley Parkway, Malvern, PA 19355, USA

(Received 6 August 1996; in revised form 1 September 1997)

Abstract—During the processing of particulate materials in rotary kilns and driers the transverse motion generated in the bed is the primary factor controlling renewal of material at the exposed bed surface. The rate of surface renewal, in turn, determines the degree of material mixing and the rate of heat transfer from the freeboard to the bed. An experimental campaign launched to investigate granular flow behavior in a transverse plane of a rotary cylinder suggests that a continuum model based on the constitutive equations developed for gravity flow in chutes may be adopted, in some particular cases, to describe flow in the shear (active) layer. A model is developed in which the dimensions of the shear layer, the region near the free surface, is assumed thin thereby permitting the governing equations to reduce to Prandtl's boundary layer equations which are solved to obtain the depth and velocity profiles within the layer. Because the density at the free surface is discontinuous for the flow regimes of practical interest, the continuum assumption breaks down at the free surface, hence, a stress-free boundary condition has been avoided. In place of this a surface velocity constraint from the experimental campaign has been applied which, therefore, makes the model deficient in exploring the full potential of the boundary layer analogy. Nevertheless, the appropriate velocity trends are predicted well into the bed with the results comparing favorably with experimental data. © 1998 Published by Elsevier Science Ltd. All rights reserved

Key Words: rotary kilns, transport phenomena, granular flows, granular temperature and granular diffusion

1. INTRODUCTION

The Processing of granular materials in rotating drums is a common industrial practice. One prominent example is the rotary kiln which is employed by industry to carry out a wide variety of processing operations; for example calcining of limestone, reduction of oxide ore, clinkering of cementitious materials, waste incineration, calcining of petroleum coke, to cite but a few. This widespread usage can be attributed to many factors the most prominent being the ability to handle varied feedstock; for example slurries or granular materials having large variations in particle size. Because of its industrial importance the rotary kiln has been the subject of numerous investigations. However, only a portion of this work has focussed on determining conditions within the bed. Thus, one avenue from which significant improvements in kiln performance might be derived is the development of a more quantitative understanding of transport phenomena within the bed material; specifically the role of momentum transport in determining the particle motion and that of kinetic energy in determining mass and energy diffusion rates. The present work focuses on the development of a model for predicting the flow of particulate materials in the transverse plane of a rotating drum of which the rotary kiln is but one example.

The transverse bed motion established in rotating drums will depend on rotation rate and the degree of fill (the portion of the drum cross-section occupied by bed material) and rheology of the particles. Several overall modes of bed motion have been identified; namely, slipping, slumping, rolling, cascading, cataracting and centrifuging (Henein *et al.* 1983a,b). Because of the need to promote good mixing of the particles along with rapid renewal of the exposed bed, the most desirable condition for industrial operations is usually the rolling mode, details of which are shown in figure 1. In this mode the bed material is characterized by two distinct regions; (1) the relatively thin active layer which is formed as granular material flows downward from the apex

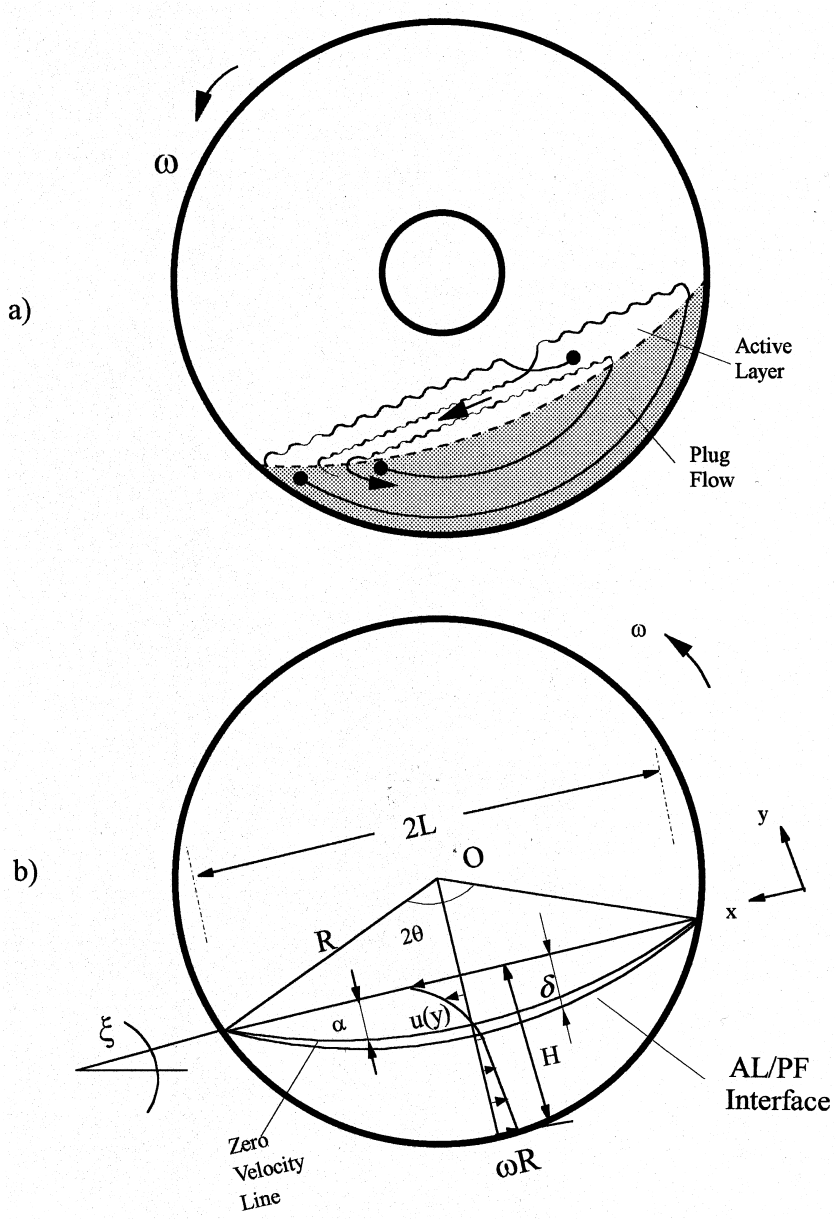

Figure 1. (a) Rolling bed motion: top plane—active (shear) layer; bottom plane—plug flow (non-shearing) region; (b) model calculation domain.

to base, and, (2) the much thicker passive (plug flow) region where the material is carried upward by the rotation of the drum. Therefore the energy imparted by the drum rotation is continuously fed into the plug flow region as potential energy which is subsequently dissipated by the vigorous interaction of particles within the active layer.

Particle velocity measurements and observations (Boateng and Barr 1997) have shown that the active layer flow encountered in rolling beds is similar, in some respect, to gravity flow in chutes. This work further showed that within most operational modes shearing and non-shearing regions can co-exist within the same flow field, thereby, indicating that stress generation may comprise a combination of static, streaming and collisional terms with the extent of each contribution depending upon material rheology and drum rotation rate. This suggests that limited application of the constitutive equations developed for cohesionless granular materials (see for example Lun *et al.* 1984; Johnson and Jackson 1987) is possible. Although other theories exist, for example plastic formulations (see, for example Mandl and Luque 1970) may be applicable

to some extent, they have not been widely tested for continuously shearing granular materials. The impetus here was to adopt specific aspects of the constitutive equations developed by Lun *et al.* (1984) and Johnson and Jackson (1987) for the boundary conditions appropriate to rotating cylinders at high shear rates. The resulting model predicts bulk flow behavior upon which rotary kiln thermal process models can draw (Boateng and Barr 1996a,b); these include: (i) the velocity field, (ii) the active layer depth, (iii) granular temperature, defined as the kinetic energy per unit mass in random motion of particles (Zhang and Campbell 1992), and (iv) mass diffusion.

2. MODEL OVERVIEW AND ASSUMPTIONS

The domain for which we seek a solution to the flow problem is depicted in figure 1. As is seen, the active layer is separated from the plug flow region by an interfacial boundary which is a few particles away from the zero velocity line. In the plug flow region particles rotate with the wall in a rigid body motion and the strain rate there is zero. Because of this rigid lattice behavior the no slippage requirement may be imposed within the plug flow region; therefore the velocity there is a linear function of radius, $u = \omega r$, and hence a solution for the flow field is only required for the active layer. Particulate flow within the active layer is rather complex and may involve all aspects of granular flow. Since the location of the interface between the plug flow region and the active layer is not known *a priori* to decouple the two flow streams one of the tasks of the model was to allow prediction of its position and hence to determine the active layer depth.

The principle assumptions necessary to model the flow were limited to the following:

(i) Particles are cohesionless, spherical, rigid, and slightly inelastic (for example, polyethylene and perhaps some processing materials).
(ii) The active layer is considered to be thin relative to the bed depth. This assumption is supported by depth probing experiments (Boateng 1993) in which the ratio of the active layer depth at mid-chord to the chord length was found to be less than 0.04.
(iii) The motion is essentially two-dimensional in the transverse plane since the transverse velocity is several orders of magnitude greater than the axial velocity.
(iv) Particle flux into the active layer in the right quadrant is assumed equal to particle flux into the plug flow region in the left quadrant; therefore only half of the two-dimensional domain is considered in the calculations (Ferron and Singh 1991).
(v) The particle ensemble behaves as a continuum and the flow properties; for example solids concentration, granular temperature, etc. are a continuous function of position. However, because the density at the free surface is discontinuous, a velocity condition from an experimental data is imposed at the free surface.
(vi) For simplicity the granular temperature in the active layer is assumed isotropic in the radial direction but varies along x.

The equations of motion describing such flows have been developed (Lun *et al.* 1984; Johnson and Jackson 1987) by considering conservation of mass, momentum and (motional) energy as

$$\frac{\partial \rho}{\partial t} + \nabla \cdot (\rho \mathbf{u}) = \mathbf{0} \qquad [1]$$

$$\rho \frac{D\mathbf{u}}{\mathrm{Dt}} = \rho \mathbf{g} - \nabla \cdot \mathbf{P} \qquad [2]$$

$$\frac{3}{2} \rho \frac{D\tilde{T}}{Dt} = -\nabla \cdot \mathbf{q}_{\mathrm{PT}} - \mathbf{P} : \nabla \mathbf{u} - \gamma \qquad [3]$$

In these expressions $\mathbf{u}$ is the bulk velocity, $\rho = \vartheta \rho_p$ is the bulk density, ϑ is the solids volume fraction and $\mathbf{P}$ is the total stress tensor, which consists of both static and kinetic (streaming and collisional) components. Johnson and Jackson (1987) have defined the term $\mathbf{q}_{\mathrm{PT}}$ as the flux of

pseudo-thermal energy and can be related to the granular temperature, $\tilde{T}$, a measure of particle kinetic energy. γ is the dissipation of pseudo-thermal energy due to inelastic collision of particles. The constitutive expressions needed for the evaluation of these terms follow Johnson and Jackson (1987) and are listed in appendix A.

Owing to the fact that material flow in a rotary drum may not be as rapid as flow in chutes, which therefore, may result in long term duration of particle interactions, the motivation was to seek thin flow approximation (boundary layer) to the governing equations and apply the stress tensor expressions developed for [2] and [3] to describe active layer flow. To fully exploit its use and to be consistent with experiment, the governing equations were cast into primitive variables as:

$$\frac{\partial u}{\partial x}+\frac{\partial v}{\partial y}=0 \tag{4}$$

$$\rho\left[u\frac{\partial u}{\partial x}+v\frac{\partial u}{\partial y}\right]=\rho g\sin\xi-\frac{\partial P_{xx}}{\partial x}-\frac{\partial P_{xy}}{\partial y} \tag{5}$$

$$\rho\left[u\frac{\partial v}{\partial x}+v\frac{\partial v}{\partial y}\right]=\rho g\cos\xi-\frac{\partial P_{xy}}{\partial x}-\frac{\partial P_{yy}}{\partial y} \tag{6}$$

$$\rho\left[u\frac{\partial \tilde{T}}{\partial x}+v\frac{\partial \tilde{T}}{\partial y}\right]=-\left[\frac{\partial q}{\partial x}+\frac{\partial q}{\partial y}\right]-\left[P_{xx}\frac{\partial u}{\partial x}+P_{xy}\frac{\partial v}{\partial x}+P_{yx}\frac{\partial u}{\partial y}+P_{yy}\frac{\partial v}{\partial y}\right]-\gamma \tag{7}$$

which can further be normalized with the appropriate scales to establish justification for the boundary layer approximation. The coordinates appropriate to the active layer may be defined in Cartesian coordinates with field variables taken with respect to x and y (figure 1) where, from assumption (iv), $0 < x < L$ and $0 < y < -\Delta$. The characteristic parameters used to normalize [4]–[7] are (see for example Savage and Hutter 1989)

$$\begin{aligned}(x,\ y)&=([L]x^*,\ [\Delta]y^*)\\ (u,\ v)&=\left([gL]^{1/2}u^*,\ \left[\frac{\Delta}{L}(gL)^{1/2}\right]v^*\right)\\ (P_{xx},\ P_{xy},\ P_{yy})&=[\cos\xi\Delta](P^*_{xx},\ P^*_{xy},\ P^*_{yy}).\end{aligned} \tag{8}$$

After this procedure (appendix B) the continuity and the momentum equations for active layer flow were obtained (dropping the asterisk) as

$$\frac{\partial u}{\partial x}+\frac{\partial v}{\partial y}=0 \tag{9}$$

$$u\frac{\partial u}{\partial x}+v\frac{\partial u}{\partial y}=\sin\xi-\sin\xi\frac{\partial P_{xy}}{\partial y} \tag{10}$$

$$\frac{\partial P_{yy}}{\partial y}=1 \tag{11}$$

For this thin flow, the y-wise momentum equation becomes the overburden, that is, $P_{yy}=\int_0^{\Delta}\vartheta\,\mathrm{d}y$. Provided that the thin flow assumption is satisfied, [9] and [10] sufficiently describe flow within this layer. However, the solution procedure for these equations can be considerably simplified if the thin flow assumption is further explored by developing the momentum equations in an integral format (see for example Schlichting 1979).

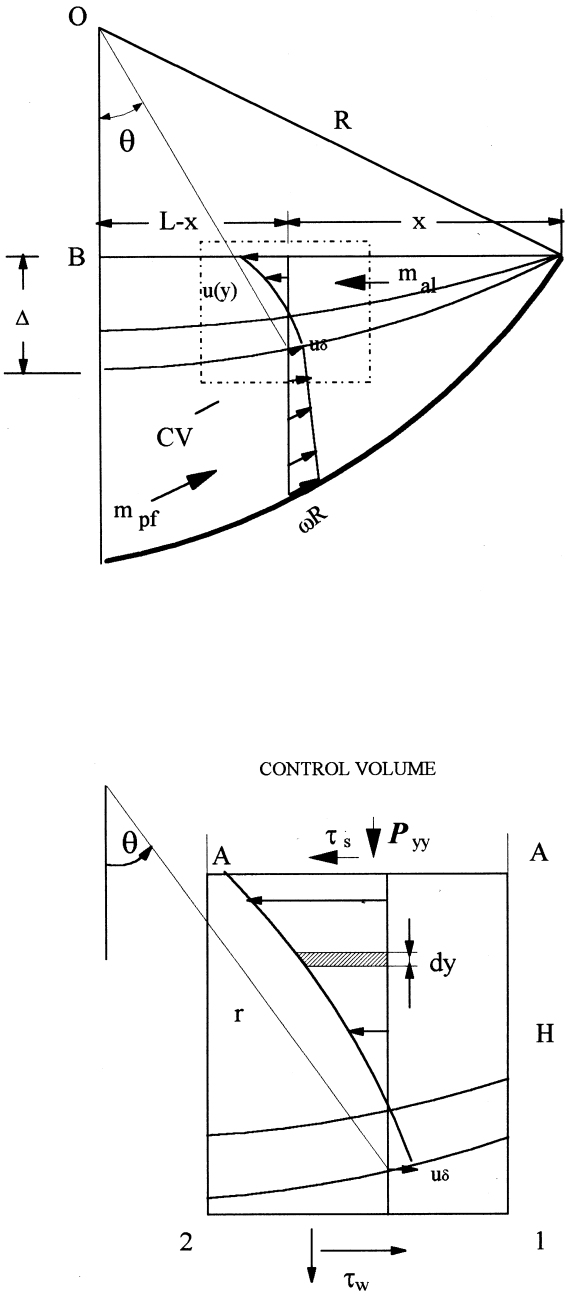

Figure 2. Schematic showing scaling variables employed in normalizing governing equations and control volume for active layer flow field.

3. INTEGRAL EQUATION FOR ACTIVE LAYER MOMENTUM CONSERVATION

It can be readily shown that by considering a control volume in the active layer (figure 2) the system of partial differential equations [9] and [10] can be reduced to a single ordinary differential equation (see for example Holman 1990) as

$$\rho \frac{\mathrm{d}}{\mathrm{d}x}\left(\int_0^H (u^2 - u_\delta u)\mathrm{d}y\right)\mathrm{d}x + \frac{\mathrm{d}u_\delta}{\mathrm{d}x}\left(\int_0^H \rho u \, \mathrm{d}y\right)\mathrm{d}x = \sum F_x \qquad [12]$$

which involves integration of certain parameters across the layer. It might also be noted that insofar as no attempt is made to describe the stress tensor nor net forces acting on the control

volume, [12] can be considered identical to one that describes conventional fluids; for example the Blasius problem (see, Schlichting 1979). In [12], u_δ, the velocity at the transition from the active layer to the plug flow, is a function of radius only ($u_\delta = \omega r_\delta$) but the radius for this location requires knowledge of the active layer depth, δ_x, at the distance, x, from the apex. Hence from the geometry of figure 2 one can show that

$$r_\delta^2 = (L - x)^2 + (OB + \delta_x)^2$$
$$\cos\theta = \frac{(OB + \delta_x)}{r_\delta} \qquad [13]$$

where OB is the distance from the cylinder centerline to the bed surface.

As was shown in [12], the net force takes on the form of the x-component of the stress generation tensor therefore,

$$\rho \frac{\mathrm{d}}{\mathrm{d}x}\left(\int_0^\Delta (u^2 - u_\delta u)\mathrm{d}y\right)\mathrm{d}x + \frac{\mathrm{d}u_\delta}{\mathrm{d}x}\left(\int_0^\Delta \rho u \,\mathrm{d}y\right)\mathrm{d}x = [-P_{xy}\,\mathrm{d}x + P_{xx}\,\mathrm{d}x_\rho g \sin\xi\,\mathrm{d}x]\Delta \qquad [14]$$

Implicit in this equation is the assumption that the top face of the control volume is a free surface for which, perhaps, a null shear stress can be applied. The second term in [14] would, in fluid flow, be equal to the hydrostatic pressure according to Bernoulli's equation. For granular flows on an incline, however, this term may be assumed equivalent to the driving force parallel to the inclined plane (subtended by the angle of repose) and hence may be equated to the overburden pressure in the x-direction, that is

$$\frac{\mathrm{d}u_\delta}{\mathrm{d}x}\int_0^\Delta \rho u \,\mathrm{d}y = P_{xx} \qquad [15]$$

which, therefore, results in an expression that describes the active layer flow as

$$\rho \frac{\mathrm{d}}{\mathrm{d}x}\int_0^\Delta (u^2 - u_\delta u)\mathrm{d}y = [\rho g \sin\xi - P_{xy}]\Delta \qquad [16]$$

The final task in this development before proceeding with a solution is to derive appropriate expressions for the shear stress acting over the bottom surface of the control volume namely P_{xy}.

As mentioned earlier, the shear stress is a combination of frictional and collisional and the extent of each contribution would be determined by operational conditions, that is the rotation rate, degree of fill of the cylinder, etc. Two regimes of operation, slumping and rolling, can be isolated for the analysis.

3.1. *Slumping bed*

When the rotation rate is low or collisions between particles are constrained and if $\partial u/\partial y > 0$ then the shear stress is strictly static which is simply given as

$$P_{xy} = \rho g \cos\xi \tan\varphi \qquad [17]$$

where φ is the static angle of repose which is not vastly different from the friction angle. This situation occurs when the active layer is not shearing by inter-particle collision. The corresponding integral-momentum equation describing slumping is, therefore,

$$\rho \frac{\mathrm{d}}{\mathrm{d}x}\int_0^\delta (u^2 - u_\delta u)\mathrm{d}y = [\rho g \sin\xi - \rho g \cos\xi \tan\varphi]\delta \qquad [18]$$

which upon rearrangement, becomes

$$\frac{\mathrm{d}}{\mathrm{d}x}\int_0^\delta (u^2 - u_\delta u)\mathrm{d}y = g\cos\xi[\tan\xi - \tan\varphi]\delta. \qquad [19]$$

Thus, if $\xi > \varphi$, the bulk bed is accelerated or it is damped when $\xi < \varphi$. When $\xi = \varphi$, it can be said that the flow is indeterminate (Kanatani 1979).

3.2. *Rolling bed*

From bed behavior experiments (Henein *et al.* 1983a), one can say that the rolling bed, with its continuous surface renewal, is a situation where kinetic stress may be the driving force for material flow. Because the material in the active layer is continuously shearing in this mode, collisional stress may dominate transfer of momentum. In this case all aspects of granular flow come into play and the shear stress may be deduced from the constitutive equations described in appendix A. Many forms of the shear stress expressions exist in the literature, however, they are all variants of the equation first proposed by Bagnold (1954) which is given as

$$P_{xy} = -c_i \rho_p \left(\mathrm{d}_p \frac{\mathrm{d}u}{\mathrm{d}y} \right)^2 \qquad [20]$$

where c_i is the Bagnold's constant (see, for example Campbell and Gong 1986). [20] may be rearranged to resemble stress/strain rate relationship as

$$P_{xy} = C' \frac{\mathrm{d}u}{\mathrm{d}y} \qquad [21]$$

where an "apparent" viscosity, C', may be defined as a function of dilation, $f(\rho_p, \mathrm{d}_p, e_p, \vartheta, \tilde{T})$. This apparent viscosity may then be related to the properties of the bed according to the relationship (see appendix A):

$$C' = -\rho_p \, \mathrm{d}_p g_2(\vartheta) \tilde{T}^{1/2} \qquad [22]$$

where $g_2(\vartheta)$ is a term in Lun *et al.* (1984) expression relating the "viscosity" to material properties such as coefficient of restitution (e_p), $\eta\{=(1 + e_p)/2\}$, the solids fraction, ϑ, and is given in the appendix A as

$$g_2(\vartheta) = \frac{5\sqrt{\pi}}{96} \left[\frac{1}{\eta(2-\eta)g_o} + \frac{8}{5}(3\eta - 1)\frac{\eta}{(2-\eta)} + \frac{64}{25}\left\{ \frac{\eta(3\eta-1)}{(2-\eta)} + \frac{12}{\pi} \right\} \vartheta^2 g_o \right] \qquad [23]$$

Near identical expressions for granular viscosity have been derived by Gidaspaw (Gidaspaw and Huilin 1996). By inserting the shear stress term into [16] the momentum conservation equation takes on its final form

$$\rho \frac{\mathrm{d}}{\mathrm{d}x} \int_0^\delta (u^2 - u_\delta u)\mathrm{d}y = [\rho \sin \xi]\delta + g_2(\vartheta)\rho_p \, \mathrm{d}_p \tilde{T}^{1/2} \frac{\mathrm{d}u}{dy}. \qquad [24]$$

It might be noted that, although the kinetic energy equation [7] has not been included explicitly in the derivation of the integral momentum equation it does appear implicitly since its solution is required in order to obtain the granular temperature in [24].

4. SOLUTION OF THE INTEGRAL MOMENTUM EQUATION IN THE ACTIVE LAYER OF A ROLLING BED

[24] represents the integro-differential equations for the bulk material flow in the bed's active layer for which a "suitable" form of the velocity profile is required to solve. In choosing this velocity function, it is necessary to account for the boundary conditions (i) at the free surface, (ii) the interface between the active layer and the plug flow region of the bed, and also to satisfy the requirement for continuity at the point where the solution in the active layer matches the plug flow solution. In addition, material balance at any arbitrary x-position on the free surface plane must be enforced. Hence a necessary constraint to effect any solution to the flow problem is to invoke assumption (iv) that is

$$\rho_{al} \int_0^{\delta_x} u_{\mathrm{al}}(x, \ y)\mathrm{d}y = \rho_{pf} \int_{r_x}^{R} u_{pf}(r)\mathrm{d}r \qquad [25]$$

Recognizing that the bulk density is simply the particle density times the solid fraction

($\rho = \rho_p \vartheta$), and that, within the plug flow region, $u = \omega r$, [25] simplifies to (dropping the subscript *al* for velocity in the active layer)

$$\vartheta_{\text{al}} \int_0^{\delta_x} u \, \mathrm{d}y = \vartheta_{pf} \int_{r_x}^{R} \omega r \, \mathrm{d}r \qquad [26]$$

which, after integration of the right hand side gives

$$\vartheta_{\text{al}} \int_0^{\delta_x} u \, \mathrm{d}y = 0.5 \vartheta_{pf} \omega \left[R^2 - \left(\frac{OB + \delta_x}{\cos\theta} \right)^2 \right] \qquad [27]$$

where $u = u_{\text{al}}(x, y) = f(y)$ is the active layer velocity function which includes the actual active layer depth. At the mid-chord, the global material balance for the entire cross-section should be satisfied and since the subtended angle there (namely, θ) goes to zero, a reduced form of [27] is equally applicable as

$$\vartheta_{\text{al}} \int_0^{\Delta} u \, \mathrm{d}y = 0.5 \vartheta_{pf} \omega [R^2 - (OB + \Delta)^2] \qquad [28]$$

Two conditions can be invoked to iteratively obtain active layer depth and velocity that is either by ensuring that the mass flow in the active layer is balanced at each x-position from the apex, using [27] (which was used as the convergence criterion), or by ensuring that global mass in the cross-section is balanced at mid-chord using [28].

Experiments (Boateng and Barr 1997) have indicated that a parabolic profile would be sufficient to describe the shape of the velocity profile in the active layer and hence three constraints may be sufficiently imposed as boundary conditions. These are described in the following two subsections.

4.1. *Free surface constraint*

Following the fluid flow analogy, the most obvious choice for a free surface boundary condition is to allow the shear stress there to vanish and thus force the shear rate to zero (namely $\mathrm{d}u/\mathrm{d}y = 0$). The boundary condition for slow and high density granular flows with free surface has been thoroughly discussed by Johnson *et al.* (1990) and also by Nott and Jackson (1992). They admit that the adoption of the stress-free surface condition for such flows gives rise to difficulties unless the free surface is considered to be at an infinite location. Although they could circumvent this physically unrealistic condition by alternative solution approaches all required knowledge of the magnitude of the combined shear stress because of the non-zero density there. In order to render their calculations strictly analytical they sought asymptotic solutions to the governing equations that matched small density values, typically, $\vartheta = 0.001$ at that infinite location. Despite its slow rate of convergence the asymptotic solution approach worked for certain inclined angles of the chute flow problem they solved. However, in the case of rotating drums, particularly for low and moderate drum speeds studied in the experimental campaign that underlies this work (Boateng and Barr 1997), this is even more difficult to apply. The reason is attributed to the fact that the flow is not as fully developed as in chute flow situations and that the weight of the particles at the exposed surface must be supported within it. The density there is comparatively greater than that encountered in rapid chute flows thereby resulting in even severe discontinuities (breakdown of the continuum assumption). Therefore the boundary condition imposed at the free surface was not that of null shear stress but rather the experimentally determined velocities (Boateng and Barr 1997). Qualitatively, the surface velocity for a bed of material of a given particle size might be expected to depend on the rotation rate, the drum size, and the degree of fill. In order to take advantage of the available data a correlation was developed relating these variables as $u_s = C_o \omega R$, where the constant of proportionality, C_o, was related to the degree of fill in percent, ϖ, and the rate of rotation of the cylinder in inverse second, ω, namely $C_o = f(\varpi, \omega)$. The relationship between C_o, at mid-chord, and the field variables for two materials are shown in figure 3.

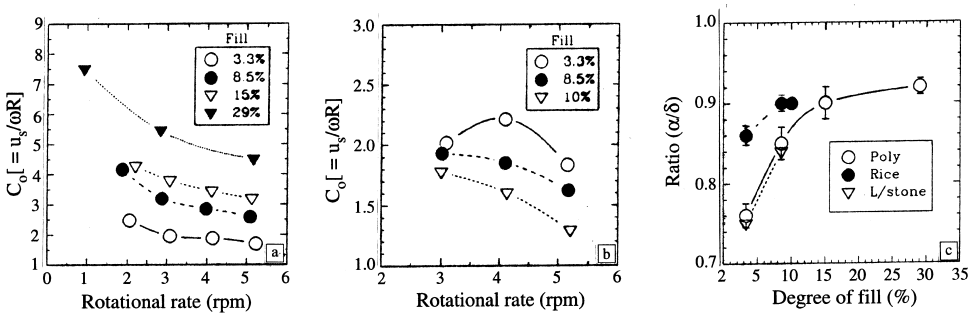

Figure 3. Experimental data for normalized surface velocity ($C_0 = u_s/\omega R$) for (a) polyethylene pellets, (b) long grain rice; (c) α/δ measured through a glass end-cap.

4.2. *Constraints for plug flow—active layer interface*

As was shown in figures 1 and 2 this interface involves both the zero velocity line (no slip), where flow reversal within the active layer occurs (distance α from the free surface) as one constraint; and the "yield" line where bed particles resume the rigid lattice structure of the plug flow region (located at distance δ from the free surface) as another constraint. The velocity condition at the point of flow reversal is simply $u = 0$ while at the yield line continuity of flow requires that $u_\delta = u_{pf}$. The relationship between α and δ may be established by considering the Coulomb yield criterion, $P_{xy} = P_{yy} \tan \xi$ which is present at all flow conditions. Since $\tan \xi$ is constant, it implies that the ratio between the shear and normal stresses at the interface must be constant. Because the normal stress is the weight of the overlying burden, the number of particles that the material can sustain between the zero velocity (no slip) line and the yield line depends on the packing and must, therefore, be related to the degree of fill. Hence, the ratio α/δ indirectly represents the yield criterion and must be a constant which is related to percent fill (drum loading). Following our thin flow analogy, this is analogous to boundary layer thickness being equal to some percentage of the free stream. Also implicit in this development is that the stress exerted by flowing granules on the passive region is equal to the limiting stress in the material as it approaches the interface. Gauthier (1991) gave a relationship of $\alpha = 0.75\delta$ for a small batch rotary drum with Ottawa sand as bed material. However, figure 3(c) suggests a value ranging between 0.7 and 0.9 with the lower values for low fill levels and tending to higher values as degree of fill increases. Although considerable scatter is present in the data, partly attributed to end-cap effects in the experimental campaign, the accuracy was considered sufficient for the modeling work.

Inclusion of these constraints into a parabolic velocity profile provides the semi-analytical expression used to describe the velocity field (appendix C) that is

$$\frac{u}{u_\delta} = \kappa + \frac{\kappa\alpha^2 - \kappa\delta^2 + \alpha}{\alpha\delta^2 - \alpha^2\delta} y + \frac{\kappa - \kappa\alpha - \alpha}{\alpha\delta^2 - \alpha^2\delta} y^2 \qquad [29]$$

where κ is the ratio between the velocity parallel to the bed surface at each x-position along the surface and the velocity at $y = \delta_x$; that is $\kappa = C_o R/r_x$. Within the bounds $0.7 < \alpha/\delta < 0.9$ the velocity profiles in the active layer can be cast into the general form,

$$\frac{u}{u_\delta} = \kappa + a_1'\left(\frac{y}{\delta}\right) - a_2'\left(\frac{y}{\delta}\right)^2 \qquad [30]$$

where the a'_i are the coefficient terms in [29] and are given in table 1. The velocity profiles obtained using [30] and depending on κ values would mimic profiles that respond to rotational rate.

In addition to the velocity profiles other parameters that are necessary in order to proceed with the solution of the momentum integral equation [24] are the density and granular temperature in the active layer. Density in the active layer will normally differ from that in the plug flow region because of increased dilation which accompanies high shear rates. In the plug flow region the solids volume concentration, ϑ_{pf}, can be assumed constant and equal to the maximum

Table 1. Coefficients for the velocity function

α/δ	a'_1	a'_2	b_0	b_1	b_2
0.75	$3.00 - 2.333\kappa$	$4.00 - 1.333\kappa$	0.170	0.422	0.033
0.80	$4.00 - 2.250\kappa$	$5.00 - 1.250\kappa$	0.177	1.875	0.000
0.85	$5.67 - 2.177\kappa$	$6.67 - 1.177\kappa$	0.093	6.768	–0.601
0.90	$9.00 - 2.111\kappa$	$10.0 - 1.111\kappa$	0.833	–0.487	–0.593

shearable solids concentration, ϑ^*, that depends on the material packing and which, in turn, depends upon the material properties, for example particle shape. For close packing of spherical particles, ϑ^* can be as high as 0.7 but as for many practical situations it ranges from 0.59–0.62 (Savage 1989). Within the active layer itself, the solids fraction can be expected to vary from that of the plug flow value ($\approx\vartheta_{pf}$) at the interface to some smaller value, ϑ_o, at the free surface because of interdependency with the granular temperature. Values of the solid fraction should, in theory, be determined as part of the solution of the granular flow equations. However, a constant value was used in the ensuing calculation because experiments (Boateng 1993) have indicated that the dilation in the active layer does not vary within 5% range and therefore little error would be incurred when a uniform value for ϑ is assumed. The same experimental work indicates that there is granular conduction into the bed. Therefore the profile for the granular temperature follows the same parabolic behavior as the velocity profile; nonetheless, it is difficult to reliably establish boundary conditions for it. Although this is not far fetched to do, it having been done in chute flow calculations, the arguments put forward to explain the granular temperature behavior at a free surface (see for example Ahn *et al.* 1991) may be inapplicable to rotary cylinders as explained earlier because only one component of $\tilde{T}$ could be measured. Therefore it was assumed that the granular temperature varied only as a function of x-position; that is, it varies only along the chord length and was computed as part of the solution of the flow problem.

Substituting the velocity profile [30] into the momentum conservation equation (the left hand side of [24]) and carrying out the integration yields the result:

$$\frac{\mathrm{d}}{\mathrm{d}x}\rho\int_0^{\delta_x}(u^2-u_\delta u)\mathrm{d}y=\rho\frac{\mathrm{d}}{\mathrm{d}x}[\{(\kappa^2-\kappa)+\tfrac{1}{2}(2\kappa a\prime_1-a\prime_1)+\tfrac{1}{3}(a\prime_1-2\kappa a\prime_1+a\prime_2)-\tfrac{1}{4}(2a\prime_1a\prime_2)+\tfrac{1}{5}a\prime_2\}\delta]u_\delta^2 \quad [31]$$

which can be substituted again into [24] to give

$$\rho\frac{\mathrm{d}}{\mathrm{d}x}[(b_0+b_1\kappa+b_2\kappa^2)\delta]u_\delta^2=\rho g\sin\xi\delta+\rho_p\,\mathrm{d}_p g_2(\vartheta)\tilde{T}^{1/2}\frac{\mathrm{d}u}{\mathrm{d}y} \quad [32]$$

where the coefficients, b_i, are the results generated when the terms in a'_i are expanded for the various values of α/δ (table 1). Again, recognizing that $\rho=\rho_p\vartheta_{al}$, [32] becomes

$$\frac{\mathrm{d}}{\mathrm{d}x}(b_0+b_1\kappa+b_2\kappa^2)\delta=\frac{g\sin\xi}{u_\delta^2}\delta+\mathrm{d}_p\frac{g_2(\vartheta)\tilde{T}^{1/1}}{\vartheta_{\mathrm{al}}\delta u_\delta} \quad [33]$$

where u_δ, the velocity in the active layer depth at distance x from apex, can be shown to be $u_\delta=-\omega(OB+\delta)$. Upon separation of the variables, [33] becomes

$$\int_0^\delta\frac{\mathrm{d}}{\mathrm{d}x}[(b_0+b_1\kappa+b_2\kappa^2)\delta]\mathrm{d}\delta=\int_0^x\left[\frac{g\sin\xi}{u_\delta^2}\delta+\mathrm{d}_p\frac{g_2(\vartheta)\tilde{T}^{1/2}}{\vartheta_{\mathrm{al}}\delta u_\delta}\right]\mathrm{d}x \quad [34]$$

Assuming a null active layer thickness at the apex; that is $\delta=0$ at $x=0$, and recognizing that $\int\delta\,\mathrm{d}\delta=\delta^2/2$ this expression takes on the quadratic form

$$\tfrac{1}{2}(b_0+b_1\kappa+b_2\kappa^2)\delta^2-\frac{g\sin\xi}{u_\delta^2}\delta x-\mathrm{d}_p\frac{g_2(\vartheta)\tilde{T}^{1/2}}{\vartheta_{\mathrm{al}}u_\delta}x=0 \quad [35]$$

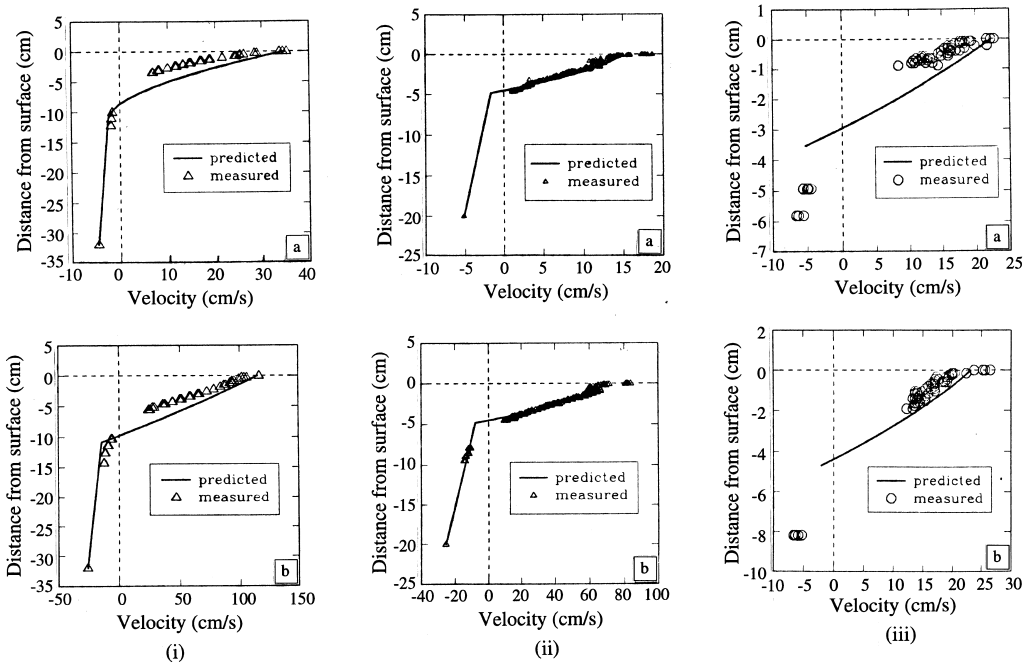

Figure 4. Predicted and measured velocity as function of radial position at mid-chord of 1 m I.D. drum for the following particle type and operating conditions: (ia) polyethylene pellets, 29% fill, 1 rpm, (ib) polyethylene pellets, 29% fill, 5 rpm; (iia) rice grains, 15% fill, 4 rpm, (iib) rice grains, 15% fill, 5 rpm; (iiia) limestone, 3.3% fill, 3 rpm (a) 3.3% fill, (iiib) limestone, 8.5% fill, 8.5%, 3 rpm.

which may be solved for the active layer depth. Once the latter is obtained, it can then be substituted into [30] to obtain the velocity distribution in the two-dimensional calculation domain. Consequently the velocity normal to the bed surface can be obtained by solving [1], the continuity equation.

The only remaining task at this point is to bring the energy equation into the solution procedure, that is to allow the granular temperature to respond to the flow [35]. The iterative technique employed to do so follows the sequence: (i) the average granular temperature, in the active layer, is guessed; with this guessed value, terms such as $g_2(\vartheta)$ are computed; (ii) as a first approximation, [35] is temporarily solved for the active layer depth, δ_x, by neglecting the quadratic term; (iii) with this value of δ_x, the velocity is determined and substituted into [35] to obtain an improved value for δ_x; (iv) using the improved δ_x, the velocity profile is obtained and the total mass flow through the active layer is determined for the current x-position; (v) this mass flow is then compared with that in the plug flow region at the same location [27]. The procedure is repeated each time bringing with it an improved estimate of the granular temperature, until the mass flow through the active layer balances the mass flow in the plug flow region to within 0.1%. Once this is accomplished the model moves on to the next x-position. Because the flow problem is assumed symmetric calculations are performed only up to the mid-chord. In performing these calculations the number of surface nodes was varied from 12 for smaller drum sizes (<0.5 m I.D.) to 24 for larger sizes (≥ 1 m I.D.). The procedure showed good numerical stability but the number of iterations required to obtain convergence, typically 50, was found to depend fairly strongly on the initial estimate supplied for the granular temperature.

5. MODEL VALIDATION AND APPLICATION

The flow model was validated against data obtained using a 1 m O.D. (96.4 cm I.D.) by 1 m long rotary drum and reported in (Boateng and Barr 1997). The results from the validation effort begin with figure 4 which shows velocities in the active layer, at mid-chord, for polyethylene pellets, rice grains and limestone at various operating conditions. These indicate a generally good agreement with experimental data, especially for lower fill levels and high rotation rates

Table 2. Model validation; AL depth at mid-chord, $(\Delta/H) \times 100\%$

Degree of fill %	Rotational rate rpm	Experimental %	Predicted %	Pershin's model %
3.3	2.05	28.57	33.24	8.33
	3.07	34.42	34.55	8.92
	4.13	36.74	35.48	10.10
	5.22	37.76	36.17	11.87
8.5	1.88	27.04	30.58	6.22
	2.87	28.48	32.15	6.64
	3.98	29.70	33.31	7.91
	5.08	31.12	34.15	8.75
15.0	2.14	23.57	28.18	4.57
	3.07	25.00	29.67	4.90
	4.11	26.29	30.86	5.89
	5.11	27.40	31.72	6.55
29.0	0.92	16.92	20.09	2.53
	2.83	18.57	25.24	3.03
	5.15	22.77	27.97	4.29

where rapid motion of particles are encountered. Discrepancies between model and experiment are only apparent in higher fill and low rotation rate test; the former can be attributed to the fact that, for deep beds, the granular temperature might not be uniform throughout the active layer at each x-position as assumed. At low shear rates, however, the flow is not entirely rapid and frictional stresses may dominate momentum generation thereby resulting in a breakdown of the collisional contribution to the stress tensor applied in the granular flow model. Nonetheless, for an approximate solution employed, the predictions are considered to be good. Although not precisely known, the coefficient of restitution for both the rice grains and the limestone are low compared with polyethylene. Based on estimated values of the coefficient of restitution (0.5 for rice and 0.6 for limestone) calculations performed using these materials do show good results as presented in the figure. It is apparent here that, with respect to predicting the gradients of the profiles, the accuracy of the predictions are comparable to those obtained for polyethylene pellets. The predictions compare well with experimental data, despite the fact that the coefficient of restitution for these materials was poorly characterized.

Active layer depths predicted at mid-chord are summarized in table 2 and compared with experimental data on polyethylene. Also presented are the results from an equilibrium model of Pershin (1988). Although Pershin performed his experiments at rotation rates close to critical values where material in the drum centrifuges that is the rotational Froude number $\mathrm{Fr} = \omega^2 R/g \rightarrow 1$, his analysis involved energy minimization that is based entirely on frictional stresses. Gauthier (1991) also carried out measurements of active layer depth for sand ($\approx$0.4 mm particles) in a 0.37 m I.D. drum and used these results to generate an empirical expression relating the depth of the active layer at mid-chord, Δ, to the bed depth at mid-chord, H, and drum speed, N. It is apparent from the table that 15% disparity exists between both models and the current one. However, both Gauthier and Pershin carried out their measurements by filming through a glass end-cap. A more detailed measurement obtained using a fibre optic technique and well away from end effects (Boateng and Barr 1997) suggests that the end-cap essentially reduces active layer depth by about 10–20%.

Having validated the model it was employed to predict the flow conditions for three rotary drums of various dimensions namely, 0.41 m I.D., applicable to pilot kilns, 1 m I.D. drum, which represents the experimental apparatus used in the model validation, and a 2.5 m I.D. drum, typical of medium size industrial processing kilns. The discussion of these predictions begins with the active layer velocity profiles and shown in figure 5. At 2 rpm, the surface velocity at mid-chord increases from 15 cm s^{-1} for the 0.41 m I.D. drum, to 40 cm s^{-1} for the 1 m I.D. drum, and then to 100 cm s^{-1} for the 2.5 m I.D. industrial size drum. At 5 rpm the respective velocities shift to a greater magnitude, namely 40 cm s^{-1}, 75 cm s^{-1}, and 200 cm s^{-1}. The results suggests a direct proportionality between surface velocity and drum size given the same operational conditions. This linear relationship responds to the boundary condition, $C_0 = u_s/\omega R$, which in turn, is related to the rotational Froude number. It might be recalled that Fr is a

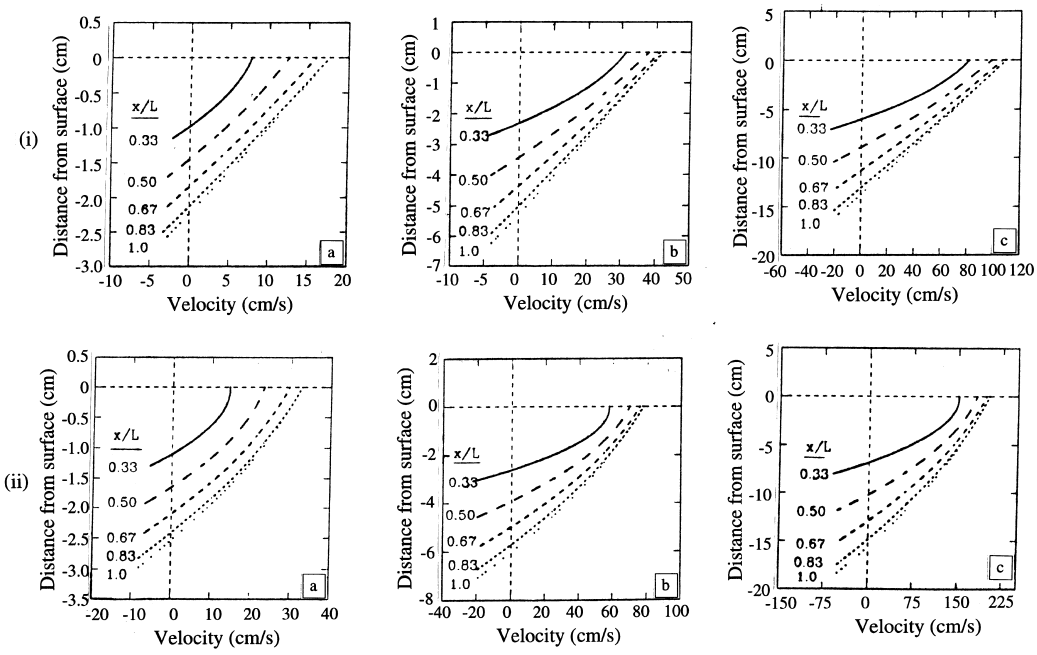

Figure 5. Predicted velocity in active layer as function of distance from apex for the following drum sizes and operating conditions: (i) 2 rpm, 12% fill; (ii) 5 rpm, 12% fill (a), (b), and (c) are respectively, 0.41 m, 1 m, and 2.5 m drum diameters.

necessary scaling parameter for rotary drums and might be used in conjunction with the model to estimate particle velocities at the free surface. Further details on the effect of drum speed and particle velocity can be revealed by considering the profiles at mid-chord as shown in figure 6. It might be noticed from the figure that the shape of the profile changes from approximately linear to parabolic with increased rotation rate. This shows the influence of shear rate on granular viscosity. One can presume that, since energy is not self sustaining in granular flows, increasing drum speed provides the necessary agitation to change the profile shape from what might be perceived as representing a Newtonian-type flow to a more dilatant-type flow. This is evident from the fuller profiles that develop as shear rate increases with rotational rate. Although not so profound this culminates to active layer growth; a result which is consistent with experimental data. Data from the experimental campaign (Boateng and Barr 1997) have shown that, when fill is held constant, the active layer thickness grows up to a well defined limit with increased rotational rate. After this limit, however, further increase in rotation rate does not draw additional material into the active layer, rather, the velocity profiles change to maintain flow continuity. It is worth noting that Couette granular flow models (Johnson and Jackson 1987) also suggested a critical speed, beyond which more material will decline to enter into the shear zone.

Another aspect of granular flow which impacts significantly on material processing operations is the granular temperature and the kinetic diffusion associated with smaller scale particle mixing. Because of assumption (vi) we discuss only the gradients in the flow direction as depicted in figure 7. These results indicate that (also see, Boateng and Barr 1997), the granular temperature increases rapidly at the onset of flow, peaks at around mid-chord, then dissipates in the flow direction. It is also expected that the granular temperature will increase with kiln speed and this is also shown in figure 7. As is seen here, the trends do follow a general granular flow behavior irrespective of the magnitude of the numerical values. The self-diffusion coefficient for equally sized particles (Ferron and Singh 1991) follow directly the same trend as the granular temperature. This self-diffusion coefficient given by the expression (Savage 1993; Hsiau and Hunt 1993)

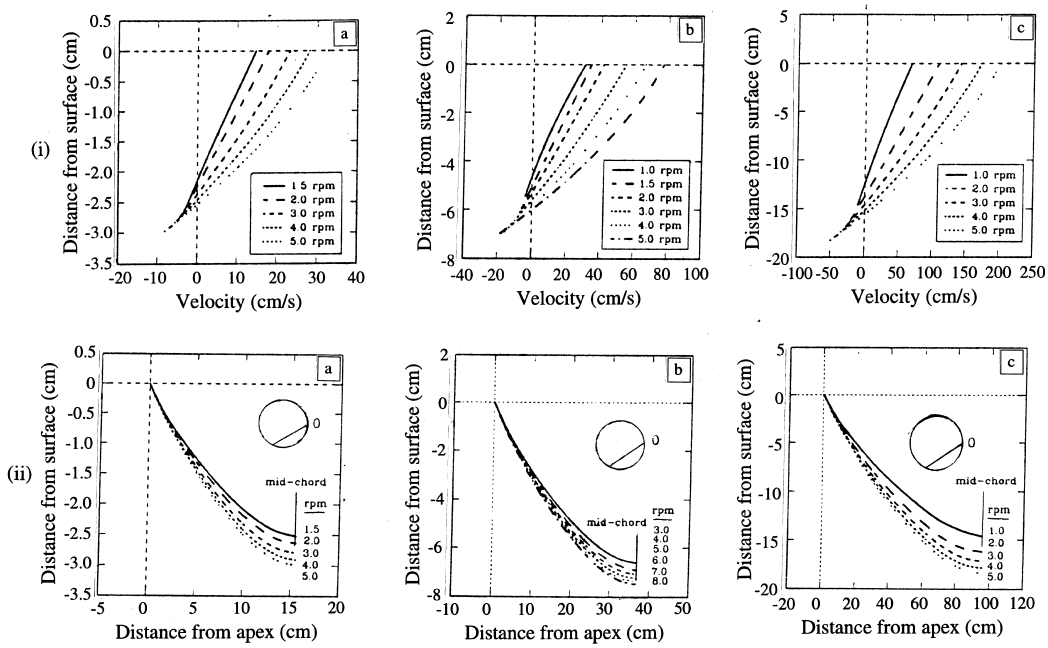

Figure 6. Predicted velocity profiles (i) and active layer depth (ii) at mid-chord as a function of rotational rate; (a), (b) and (c) are drum diameters of 0.41 m, 1 m drum, and 2.5 m.

$$\tilde{D} = \frac{d_p\sqrt{\pi\tilde{T}}}{8(e_p+1)\vartheta g_0(\vartheta)}, \qquad [36]$$

is inversely proportional to the coefficient of restitution of particles and solid concentration, but directly proportional to the square root of the granular temperature. Therefore, when the material type and solids concentration are held constant, diffusion rates can be expected to increase with granular temperature and rotation rate (figure 8). This result is of special importance to material processing in rotary drums for the simple reason that, if the bulk velocity in the flow direction is considered convective, then it is the small scale particle diffusion which is responsible for mixing and hence thermodynamic temperature uniformity.

The results presented thus far have been confined to the effects of rotation rate and degree of fill on the particle flow. However the effects of the physical properties of the material (material type), specifically the solids concentration, coefficient of restitution and the angle of repose, on

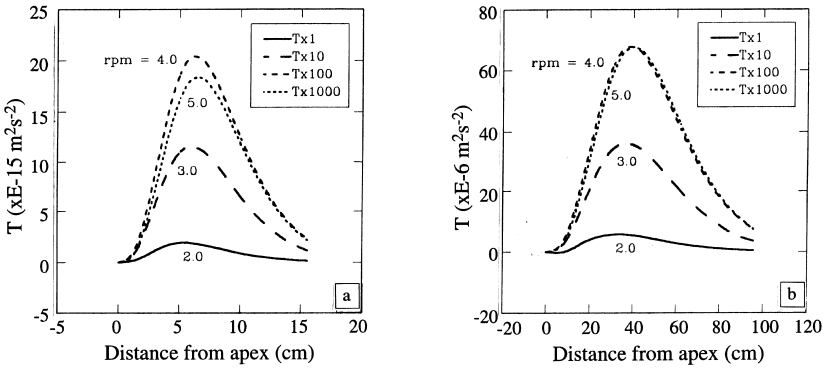

Figure 7. Predicted granular temperature as function of rotational rate for the following conditions: (a) 0.41 m drum, 12% fill; (b) 2.5 m drum, 12% fill.

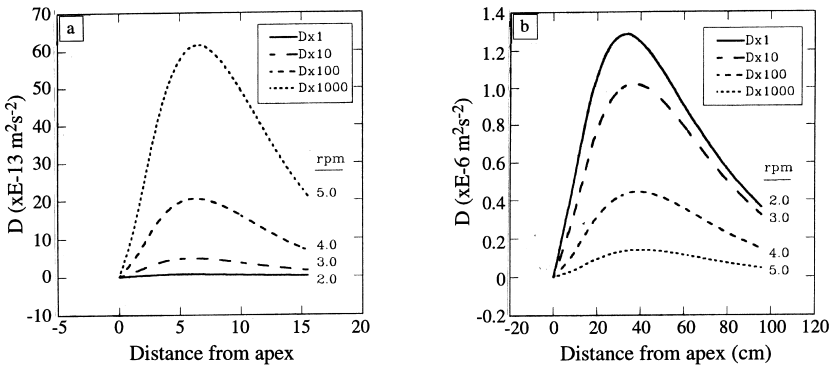

Figure 8. Predicted kinetic diffusion as function of rotational rate for the following conditions: (a) 0.41 m drum, 12% fill; (b) 2.5 m drum, 12% fill.

flow characteristics were also explored using the model. Since the solids concentration is a measure of dilation and hence, the state of fluidization or expansion of the bed burden, it might be expected to significantly influence the flow behavior. The model predictions shown in figure 9 indicate that, as the dilation of the bed increases, the quantity of the material entering the sheared region, that is the active layer also increases as is expected. The increased content of the active layer which is induced by dilation is reflected in an increase in the depth of the shear layer and is sufficient to cause a decline in mean shear rates present. The overall effect of this modest dilation (10% increment) is responsible for an increase in material diffusion by tenfold. Bearing in mind that most chemical reactions take place in the active layer the effect of density on material processing should not be underestimated.

On the coefficient of restitution, one can say that it is a measure of the particle's ability to retain kinetic energy during collisions and hence higher values will tend to reduce energy dissipation due to inelastic collisions (Mohan *et al.* 1997). Therefore, for a fixed concentration, the granular temperature is likely to increase as is depicted in figure 10. Sensitivity analysis indicates that increasing the coefficient of restitution by 10 percentage points (in the lower range of e_p) results in over 40% increase in granular temperature. However, this effect significantly reduces at the higher range of e_p, that is near the perfect elastic limit ($e_p = 1$). The angle of repose differs only slightly from the friction angle of the material. Therefore material with higher angle of repose is expected to increase energy dissipation due to inelastic collision and frictional contribution to the stress generation will dominate flow and slumping of the bed will result.

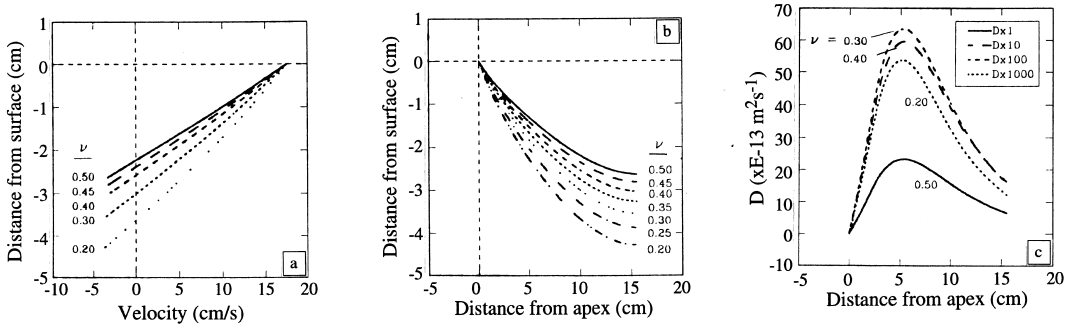

Figure 9. Effect of solids concentration on the flow character in a 0.4 m drum operating at 12% fill and 2 rpm: (a) velocity profiles, (b) active layer depth, and (c) kinetic diffusion.

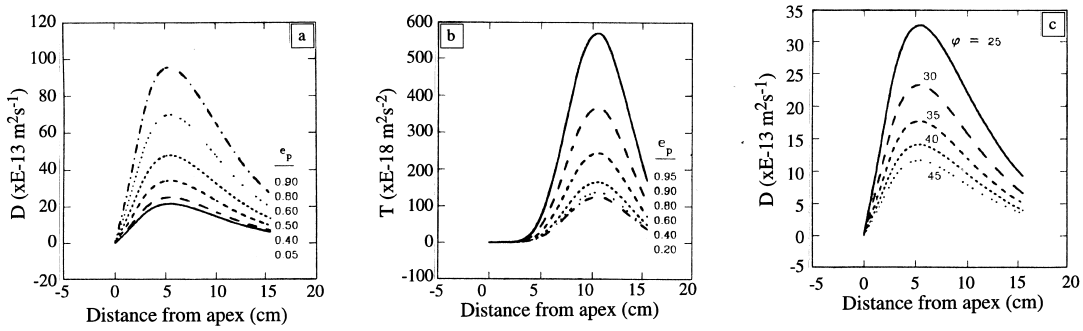

Figure 10. Effect of coefficient of restitution on flow character in a 0.41 m drum operating at 12% fill and 2 rpm: (a) diffusion, (b) granular temperature; (c) effect of static angle of repose.

6. MODEL PREDICTION FOR FLOW IN THE TRANSVERSE PLANE

To this stage the focus has been on the development of means to predict the extent of the active layer along with various flow parameters within this region. In doing so full use has been made of the relative thinness of the active layer (compared with the plug flow region) in order to develop the flow expressions on the basis of the techniques developed for other thin flows. However, the application most useful to industry is the prediction of the flow field for the transverse plane in its entirety that is, inclusive of the plug flow region. It is only by doing so that the flow field can be incorporated into existing thermal models (Barr *et al.* 1989) which have been, necessarily, based on the assumption of complete mixing over the transverse plane; that is well mixed bed. To predict the transverse flow field we first establish the extent of the plug flow region by determining the domain of the active layer using the model described. Then the grid for the computational domain is re-meshed to include the plug flow region where material follows rigid lattice motion. To be consistent with the latter, particle velocities in the plug flow region are computed as a linear function of the rotational rate and radius. Within the active layer itself, the components of the velocity vector normal to the bed surface, although small, were computed using a backward-difference formulation of the continuity equation.

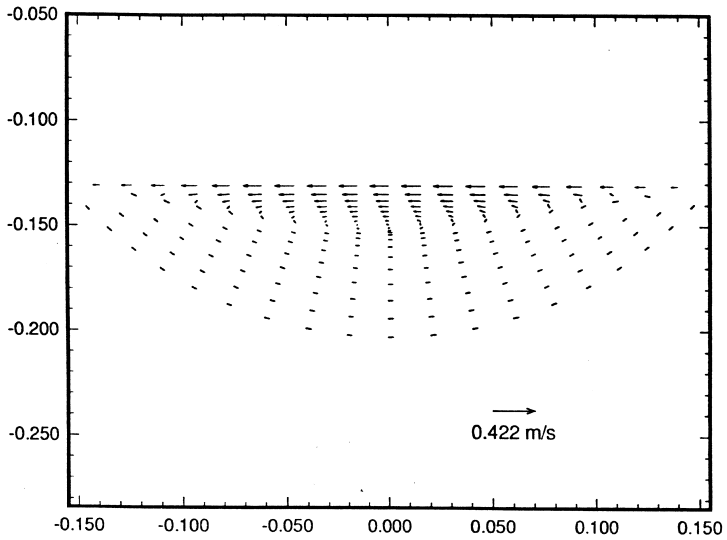

Figure 11. Predicted velocity field for 0.41 m drum cross-section with polyethylene as granular material operating at 12% fill and 2 rpm.

Model predictions for a 0.41 m I.D. drum operating at 12% fill ($\varpi = 12$) and 2 rpm ($\omega = 0.21$) are presented in figure 11. As this example shows, the continuous furnishing of material from the plug flow region into the active layer (and vice versa) can be captured by the model. By following a single particle in its journey through the active layer one can observe that, after emerging from the plug flow region near the apex, the individual particle will accelerate downward in a stream of particles which form the active layer. For low shear rates where collision contribution to momentum transport is small particles follow fixed paths practical ramifications of which is segregation or de-mixing (Boateng and Barr 1996a). At high shear rates particle contact time is short and granular temperature increases; this results in increased diffusion; its practical ramification is that each particle has an equal chance of being anywhere in the active layer thereby resulting in bed mixing followed by temperature uniformity in heat transfer modeling (Boateng and Barr 1996b; Boateng *et al*. 1997).

7. CONCLUSIONS

As part of an effort to improve our predictive capabilities for rotary kiln processes a mathematical model based on the continuum flow of bulk solids was developed to predict the velocity field established by particle motion in the transverse plane of a rotating cylinder. The model is simplified by adopting the thin flow analogy for conventional fluids and is capable of determining, in addition to the velocity, important flow parameters such as granular temperature and flow-induced kinetic diffusion.

It can be concluded that the dilation factor exhibits a strong dependence on the flow behavior and that the relationship between the shear rate and the shear stress varies with respect to dilation. By increasing the rotation rate velocity profiles can develop into shapes which mimic, progressively, pseudoplastic (root), Newtonian (linear), and dilatant (quadratic) flow behavior. These are accompanied by systematic increase in granular temperature and hence radial diffusion. The analysis shows that the material's coefficient of restitution does not dramatically influence the bulk velocity of particles but, rather, increases kinetic energy by increasing small scale velocity fluctuations as reflected in the increase in the granular temperature and increased kinetic diffusion. The foregoing analyses indicate that diffusion (radial or axial) and hence flow-induced kinetic mixing would be high in industrial rotary kilns operating at elevated rotational rates and at low degrees of fill. This condition will pertain to greater active layer depths which are necessary for material processing in continuous rotary kiln reactors provided the residence time for the particular process is not compromised.

REFERENCES

Ahn, H., Brennen, C. E. and Sabersky, R. H. (1991) Measurements of velocity, velocity fluctuation, density, and stresses in chute flows of granular materials. *J. Applied Mech.* **58,** 792–803.

Bagnold, R. A. (1954) Experiments on a gravity-free dispersion of large solids spheres in a newtonian fluid under shear. *Proc. Royal Soc. London* **A225,** 49–63.

Boateng, A. A. (1993) Rotary kiln transport phenomena: study of the bed motion and heat transfer, *Ph.D Dissertation,* University of British Columbia, Vancouver.

Boateng, A. A. and Barr, P. V. (1996a) Modelling of particle mixing and segregation in the transfer plane of a rotary kiln. *Chem. Eng. Sci.* **51,** 4167–4181.

Boateng, A. A. and Barr, P. V. (1996b) A thermal model for the rotary kiln including heat transfer within the bed. *Int. J. Heat Mass Transfer* **39,** 2131–2147.

Boateng, A. A. and Barr, P. V. (1997) Granular flow behaviour in the transverse plane of a partially filled rotating cylinder. *J. Fluid Mech.* **330,** 233–249.

Boateng, A. A., Thoen, E. R. and Orthlieb, F. L. (1997) Modeling the pyroprocess kinetics of shale expansion in a rotary kiln. *Trans. IChemE. Chem. Eng. Res. & Des.* **75,** 278–283.

Barr, P. V., Brimacombe, J. K. and Watkinson, A. P. (1989) A heat-transfer model for the rotary kiln, part II: development of the cross-section model. *Met. Trans. B.* **20B,** 403–415.
Campbell, C. S. and Gong, A. (1986) The stress tensor in a two-dimensional granular shear flow. *J. Fluid Mech.* **164,** 107–125.
Ferron, J. R. and Singh, D. K. (1991) Rotary kiln transport processes. *AIChE J.* **37,** 758–774.
Gauthier, C. (1991) Etude du movement granulaire dans cylindre en rotation. *M.Sc Thesis*, Universite du Quebec a Chicoutimi, Canada.
Gidaspow, D. and Huilin, L. (1996) Collisional viscosity of FCC particles in a CFB. *AIChE J.* **42,** 2503–2510.
Henein, H., Brimacombe, J. K. and Watkinson, A. P. (1983a) Experimental study of transverse bed Motion in rotary kilns. *Met. Trans. B.* **14B,** 191–205.
Henein, H., Brimacombe, J. K. and Watkinson, A. P. (1983b) The modelling of transverse solids motion in rotary kilns. *Met. Trans. B.* **14B,** 207–220.
Hsiau, S. S. and Hunt, M. L. (1993) Kinetic theory analysis of flow-induced particle diffusion and thermal conduction in granular material flows. *J. Heat Transfer* **115,** 541–548.
Holman, J. P. (1990) *Heat Transfer*, 7th edn. McGraw-Hill, New York.
Kanatani, K. (1979) A continuum theory for the flow of granular materials. *J. Theoretical & Applied Mech.* **27,** 571–578.
Johnson, P. C. and Jackson, R. (1987) Frictional-collisional constitutive relations for granular materials with application to plane shearing. *J. Fluid Mech.* **176,** 67–93.
Johnson, P. C., Nott, P. and Jackson, R. (1990) Frictional-collisional equations of motion for particulate flows and their application to chutes. *J. Fluid Mech.* **210,** 501–535.
Lun, C. K. K., Savage, S. B., Jeffrey, D. J. and Chepurniy, N. (1984) Kinetic theories for granular flow: inelastic particles in couette flow and slightly inelastic particles in a general flowfield. *J. Fluid Mech.* **140,** 223–256.
Mandl, G. and Luque, R. F. (1970) Fully developed plastic shear flow of granular materials. *Geotechnique* **20,** 277–307.
Mohan, L. S., Nott, P. R. and Rao, K. K. (1997) Fully developed flow of coarse granular materials through a vertical channel. *Chem. Eng. Sci.* **52,** 913–933.
Nott, P. and Jackson, R. (1992) Frictional-collisional equations of motion for granular materials and their application to flow in aerated chutes. *J. Fluid Mech.* **241,** 125–144.
Pershin, V. F. (1988) Energy method for describing granular motion in a smooth rotating cylinder. *Teoreticheskie Osnovy Khimicheskoi Tekhnologii* **22,** 255–260.
Savage, S. B. and Jeffrey, D. J. (1981) The stress tensor in a granular flow at high shear rates. *J. Fluid Mech.* **110,** 225–272.
Savage, S. B. (1989) Granular flow materials. In *Theoretical and Applied Mechanics*, ed. P. Germain, M. Piau and D. Caillerie, pp. 241–266. Elsevier, Amsterdam.
Savage, S. B. (1993) Disorder diffusion and structure formation in granular flows. In *Disorder and Granular Media*, ed. D. Bideau. Elsevier, Amsterdam.
Savage, S. B. and Hutter, K. (1989) The motion of a finite mass of granular material down a rough incline. *J. Fluid Mech.* **199,** 177–215.
Schlichting, H. (1979) *Boundary-Layer Theory*. McGraw-Hill, New York.
Zhang, Y. and Campbell, C. S. (1992) The interface between fluid-like and solid-like behavior in two-dimensional granular flows. *J. Fluid Mech.* **237,** 541–568.

APPENDIX A. GRANULAR FLOW EQUATIONS OF MOTION

In the equations of motion ([1]–[3]) the kinetic contribution to the stress tensor may be given following Lun *et al.* (1984) as

$$\mathbf{P} = [\rho\tilde{T}(1 + 4\eta\vartheta g)_0) - \eta\mu_b\nabla\cdot\mathbf{u}]\mathbf{I} - \left\{\frac{2\mu}{\eta(2-\eta)g_0}\left(1+\frac{8}{5}\eta\vartheta g_0\right)\left[1+\frac{8}{5}\eta(3\eta-2)\vartheta g_0\right]+\frac{6}{5}\mu_b\eta\right\}\mathbf{S} \quad [37]$$

the equation having been derived by considering pair distribution function in collision theory. $\mathbf{S}$ is the deviatoric stress which is expressed as

$$\mathbf{S} = \tfrac{1}{2}(\mathbf{u}_{i,j} + \mathbf{u}_{j,i}) - \tfrac{1}{3}\mathbf{u}_{k,k}\delta_{ij} \quad [38]$$

where δ_{ij} is the kronecker delta; that is, $\delta_{ij}=1$ for $i = j$, $\delta_{ij}=0$ for $i \neq j$. The flux term for pseudo-thermal energy may also be evaluated using (Johnson and Jackson 1987)

$$\mathbf{q}_{\mathrm{PT}} = -\frac{\lambda_i}{g_0}\left\{\left(1+\frac{12}{5}\eta\vartheta g_0\right)\left[1+\frac{12}{5}\eta^2(4\eta-3)\vartheta g_0\right]+\frac{64}{25\pi}(41-33\eta)(\eta\vartheta g_0)^2\right\}\nabla\tilde{T} - \frac{\lambda_i}{g_0}\left(1+\frac{12}{5}\eta\vartheta g_0\right)\frac{12}{5}\eta(2\eta-1)(\eta-1)\frac{\mathrm{d}}{\mathrm{d}\vartheta}(\vartheta^2 g_0)\frac{\tilde{T}}{\vartheta}\nabla\vartheta \quad [39]$$

with the dissipation of energy due to inelastic collisions expressed as

$$\gamma = \frac{48}{\sqrt{\pi}}\eta(1-\eta\rho_p)\frac{\vartheta^2}{\mathrm{d}_p}\tilde{T}^{3/2} \quad [40]$$

In the forgoing, μ_b is the bulk "viscosity" for perfectly elastic particles and $\eta\mu_b$ is the bulk "viscosity" for inelastic particles. λ is the granular conductivity and λ_i is the granular conductivity for inelastic particles. η is the average value between the coefficient of restitution of particles, e_p, and that of a perfectly elastic particle which has $e_p=1$. μ is the shear viscosity which depends on the mass, m, and particle diameter d_p. μ_i is therefore the shear viscosity for inelastic particles. Finally, g_0 is the radial distribution function at contact during collisions which relates the solids volume fraction, ϑ, and the maximum shearable volume fraction, ϑ^*. Pertinent definitions are summed up as follows:

$$\lambda = \frac{75m\sqrt{\frac{\tilde{T}}{\pi}}}{64\,\mathrm{d}_p^2} \qquad \mu = \frac{5m\sqrt{\frac{\tilde{T}}{\pi}}}{16\,\mathrm{d}_p^2}$$

$$\lambda_i = \frac{8\lambda}{\eta(41-33\eta)} \qquad \mu_i = \frac{\mu}{\eta(2-\eta)} \quad [41]$$

$$\eta = \frac{1}{2}(1+e_p) \qquad \mu_b = \frac{256\mu\vartheta^2 g_0}{5\pi}$$

The apparent viscosity term C' employed in the momentum equation is hence derived in terms of the coefficient of restitution of the particles, solids concentration, particle size, and granular temperature if it is recalled that the shear stress term in the momentum equation is represented as

$$P_{xy} = \frac{\partial}{\partial y}\left(C'\frac{\partial u}{\partial y}\right). \quad [42]$$

Hence, $C' = C/2$ may be deduced from the constitutive equations for slightly inelastic particle collisions (Lun *et al.* 1984) where

$$C = \frac{2\mu}{\eta(2-\eta)g_0}\left(1+\frac{8}{5}\eta\vartheta g_0\right)\left[1+\frac{8}{5}\eta(3\eta-2)\vartheta g_0\right]+\frac{6}{5}\mu_b\eta \quad [43]$$

Therefore, C' can be written as

$$C' = -\rho_p\,\mathrm{d}_p g_2(\vartheta)\tilde{T}^{1/2} \quad [44]$$

with

$$g_2(\vartheta) = \frac{5\sqrt{\pi}}{96}\left[\frac{1}{\eta(2-\eta)g_0} + \frac{8}{5}(3\eta-1)\frac{\vartheta}{(2-\eta} + \frac{64}{25}\left\{\frac{\eta(3\eta-1)}{(2-\eta)} + \frac{12}{\pi}\right\}\vartheta^2 g_0 \quad [45]$$

Similarly,

$$P_{xx} = P_{xy} - \rho_p g_1(\vartheta,\ e_p)\tilde{T} \quad [46]$$

$$q_y = -\rho_p d_p\left(g_3(\vartheta,\ e_p)\tilde{T}^{1/2}\frac{\mathrm{d}\tilde{T}}{\mathrm{d}y} + g_4(\vartheta,\ e_p)\tilde{T}^{1/2}\frac{\mathrm{d}\vartheta}{\mathrm{d}y}\right) \quad [47]$$

$$\gamma = \frac{\rho_p}{d_p}g_5(\vartheta,\ e_p)\tilde{T}^{3/2} \quad [48]$$

where g_0, g_1, g_2, g_3, g_4 and g_5 follow Johnson and Jackson (1987) as follows:

$$\begin{aligned}
g_0 &= \left(1 - \frac{\vartheta}{\vartheta^*}\right)^{-1/3}\\
g_1 &= \frac{5\sqrt{\pi}}{96}\left[\frac{1}{\eta(2-\eta)g_0(\vartheta)} + \frac{8}{5}\frac{(3\eta-1)}{5(2-\eta)\vartheta} + \frac{64}{25}\eta\left\{\frac{(3\eta-2)}{(2-\eta)} + \frac{12}{\pi}\right\}\eta^2 g_0(\vartheta)\right]\\
g_2 &= \frac{5\sqrt{\pi}}{96}\left[\frac{1}{\eta(2-\eta)g_0} + \frac{8}{5}(3\eta-1)\frac{\vartheta}{(2-\eta)} + \frac{64}{25}\left\{\frac{\eta(3\eta-1)}{(2-\eta)} + \frac{12}{\pi}\right\}\vartheta^2 g_0\right]\\
g_3 &= \frac{25\pi}{16\eta(41-33\eta)}\left[\frac{1}{g_0} + \frac{12}{5\eta}\{1+\eta-3)\}\eta + \frac{16}{25\eta^2}\left\{9\eta(4\eta-3) + \frac{4}{\pi}(41-33\eta)\right\}\vartheta^2 g_0(\vartheta)\right]\\
g_4 &= \frac{15\sqrt{\pi}}{4}\frac{(2\eta-1)(\eta-1)}{(41-33\eta)}\left(\frac{1}{g_0(\vartheta)} + \frac{12\eta}{5}\right)\frac{\mathrm{d}}{\mathrm{d}\vartheta}\{\vartheta^2 g_0(\vartheta)\}\\
g_5 &= \frac{48}{\sqrt{\pi}}\,\eta\,(1-\eta)\,\vartheta^2 g_0
\end{aligned} \quad [49]$$

APPENDIX B. NORMALIZATION OF THE EQUATIONS OF MOTION

In order to apply boundary layer solution to the active layer flow it is important to perform an order of magnitude analysis so as to establish which of the terms in the equation will vanish for thin flows. This was done by normalizing the equations with the following scaling parameters:

$$\begin{aligned}
(x,\ y) &= ([L]x^*,\ [\Delta]y^*)\\
(u,\ v) &= \left([gL]^{1/2}u^*,\ \left[\frac{\Delta}{L}(gL)^{1/2}\right]v^*\right)\\
(P_{xx},\ P_{xy},\ P_{yy}) &= [\rho g\cos\xi\Delta](P^*_{xx},\ P^*_{xy},\ P^*_{yy})
\end{aligned} \quad [50]$$

Substituting these parameters into the equations of motion would yield the following:

(i) Continuity equation:

$$\frac{\partial[(gL)^{1/2}]u^*}{\partial[L]x^*} + \frac{\partial[\frac{\Delta}{L}(gL)^{1/2}]v^*}{\partial[\Delta]y^*} = 0 \quad [51]$$

which may be rearranged to give

$$\frac{(gL)^{1/2}}{L}\frac{\partial u^*}{\partial x^*}+\frac{(gL)^{1/2}\Delta}{\Delta L}\frac{\partial v^*}{\partial y^*}=0. \quad [52]$$

Upon recognizing that

$$\frac{(gL)^{1/2}}{L}\times\frac{\Delta L}{(gL)^{1/2}\Delta}=1 \quad [53]$$

the continuity equation becomes

$$\frac{\partial u^*}{\partial x^*}+\frac{\partial v^*}{\partial y^*}=0. \quad [54]$$

(ii) The x-wise momentum equation:

$$\rho(gL)^{1/2}u^*\frac{\partial[(gL)^{1/2}u^*]}{\partial[L]x^*}+\rho\left\{\frac{\Delta}{L}(gL)^{1/2}\right\}v^*\frac{\partial[(gL)^{1/2}u^*]}{\partial[\Delta]y^*}=\rho\sin\xi-\frac{\partial[\cos\xi]P^*_{xx}}{\partial[L]x^*}-\frac{\partial[\cos\xi\Delta]P^*_{xx}\tan\xi}{\partial[\Delta]y^*} \quad [55]$$

which, upon rearranging, yields

$$\rho\frac{(gL)^{1/2}\cdot(gL)^{1/2}}{L}u^*\frac{\partial u^*}{\partial x^*}+\rho\frac{\frac{\Delta}{L}(gL)^{1/2}\cdot(gL)^{1/2}}{\Delta}v^*\frac{\partial u^*}{\partial y^*}=\rho g\sin\xi-\rho g\cos\xi\frac{\Delta}{L}\frac{\partial P^*_{xx}}{\partial x^*}-\rho g\cos\xi\tan\xi\frac{\partial P^*_{xy}}{\partial y^*}. \quad [56]$$

By making the substitution $\boldsymbol{\varepsilon}=\boldsymbol{\Delta}/\boldsymbol{L}$, and dividing by $\boldsymbol{\rho g}$, the equation reduces to

$$u^*\frac{\partial u^*}{\partial x^*}+v^*\frac{\partial u^*}{\partial y^*}=\sin\xi-\epsilon\cos\xi\frac{\partial P^*_{xx}}{\partial x^*}-\sin\xi\frac{\partial P^*_{xy}}{\partial y^*} \quad [57]$$

(iii) The y-wise momentum equation:

Similarly, the y-wise momentum follows as

$$\rho(gL)^{1/2}u^*\frac{\partial\left[\frac{\Delta}{L}(gL)^{1/2}\right]v^*}{\partial[L]x^*}+\left\{\frac{\Delta}{L}(gL)^{1/2}\right\}v^*\frac{\partial\left[\frac{\Delta}{L}(gL)^{1/2}\right]v^*}{\partial[\Delta]y^*}=-\rho g\cos\xi-\frac{\rho g\cos\xi\tan\xi\Delta}{L}\frac{\partial P^*_{xy}}{\partial x^*}-\frac{\rho\cos\xi\Delta}{\Delta}\frac{\partial P^*_{yy}}{\partial y^*} \quad [58]$$

which is rearranged to give

$$\left[\rho(gL)^{1/2}\frac{\Delta}{L}\frac{(gL)^{1/2}}{L}\right]u^*\frac{\partial v^*}{\partial x^*}+\left[\rho\frac{\Delta}{L}(gL)^{1/2}\cdot\frac{\Delta}{L\Delta}\right]v^*\frac{\partial v^*}{\partial y^*}=\rho g\cos\xi-\rho g\cos\xi\tan\xi\frac{\Delta}{L}\frac{\partial P^*_{xx}}{\partial x^*}-\rho g\cos\xi\frac{\partial P^*_{yy}}{\partial y^*}. \quad [59]$$

and is subsequently reduced to

$$\varepsilon\left[u^*\frac{\partial v^*}{\partial x^*}+v^*\frac{\partial v^*}{\partial y^*}\right]=-\cos\xi-\epsilon\cos\xi\tan\xi\frac{\partial P^*_{xy}}{\partial x^*}-\cos\xi\frac{\partial P^*_{yy}}{\partial y^*} \quad [60]$$

Recognizing that the active layer depth, even at mid-chord, is only a few particles away the terms involving ε may be small compared with the rest. Therefore, as $\varepsilon\to 0$, the equations of motion become

$$\frac{\partial u^*}{\partial x^*} + \frac{\partial v^*}{\partial y^*} = 0$$
$$u^* \frac{\partial u^*}{\partial x^*} + v^* \frac{\partial u^*}{\partial y^*} = \sin\xi - \sin\xi \frac{\partial P^*_{xy}}{\partial y^*} \quad [61]$$
$$\frac{\partial P^*_{yy}}{\partial y^*} = 1$$

Appendix C. Velocity Profile For Active Layer Flow

The velocity function employed and the appropriate boundary conditions are as follows:

$$\begin{aligned} u &= a_0 + a_1 y + a_2 y^2 \\ y &= \alpha,\ u = 0 \\ y &= \delta,\ u = u_\delta \\ y &= 0,\ u = u_s \end{aligned} \quad [62]$$

upon substituting the boundary conditions a set of algebraic equations evolve as

$$\begin{aligned} u_s &= a_0 \\ 0 &= a_0 + a_1\alpha + a_2\alpha^2 \\ -u_\delta &= a_0 + a_1\delta + a_2\delta^2 \end{aligned} \quad [63]$$

which can be reduced to two equations i.e.,

$$\begin{aligned} a_1\alpha\delta + a_2\alpha^2\delta &= -u_s\delta \\ a_1\alpha\delta + a_2\alpha\delta^2 &= -(u_s + u_\delta)\alpha \end{aligned} \quad [64]$$

and for which $\boldsymbol{a}_1$ and $\boldsymbol{a}_2$ represent

$$\begin{aligned} a_1 &= \frac{-u_s\delta^2 + (u_s + u_\delta)\alpha^2}{\alpha\delta^2 - \alpha^2\delta} \\ a_2 &= \frac{u_s\delta - (u_s + u_\delta\alpha}{\alpha\delta^2 - \alpha^2\delta} \end{aligned} \quad [65]$$

Substituting $\boldsymbol{a}_0$, $\boldsymbol{a}_1$, and $\boldsymbol{a}_2$ into the velocity profile yields

$$u = u_s + \frac{u_s(\alpha^2 - \delta^2) + u_\delta\alpha^2}{\alpha\delta^2 - \alpha^2\delta} y + \frac{u_s(\delta - \alpha) - u_\delta\alpha}{\alpha\delta^2 - \alpha^2\delta} y^2. \quad [66]$$

It may be recognized that $\boldsymbol{u_s} = \boldsymbol{C}_0\boldsymbol{\omega R}$ and $\boldsymbol{u_\delta} = \boldsymbol{\omega r_x}$, and hence $\boldsymbol{u_s}$ can be expressed as a ratio

$$u_s = \frac{C_0 R}{r_x} u_\delta = \kappa u_\delta \quad [67]$$

which, upon substitution into the velocity function yields

$$\frac{u}{u_\delta} = \kappa + \frac{\kappa\alpha^2 - \kappa\delta^2 + \alpha}{\alpha\delta^2 - \alpha^2\delta} y + \frac{\kappa - \kappa\alpha - \alpha}{\alpha\delta^2 - \alpha^2\delta} y^2. \quad [68]$$

For example, if $\boldsymbol{\alpha} = 0.75\boldsymbol{\delta}$ is substituted into the preceding equation, then the velocity profile will take on the form

$$\frac{u}{u_\delta} = \kappa + (3 - 2.33\kappa)\left(\frac{y}{\delta}\right) - (4 - 1.33\kappa)\left(\frac{y}{\delta}\right)^2 \quad [69]$$

or

$$\frac{u}{u_\delta} = \kappa + a\prime_1\left(\frac{y}{\delta}\right) - a\prime_2\left(\frac{y}{\delta}\right)^2 \quad [70]$$

as given in the text.